



Macroscale vertical power-law distribution of bacteria in dark oceans can emerge from microscale bacteria-particle interactions

Takeshi Miki^{a,b,c,*}, Po-Ju Ke^{d,b}

^a Faculty of Advanced Science and Technology, Ryukoku University, Otsu, Shiga 520-2194, Japan

^b Institute of Oceanography, National Taiwan University, Taipei 10617, Taiwan

^c Center for Biodiversity Science, Ryukoku University, Otsu, Shiga 520-2194, Japan

^d Institute of Ecology and Evolutionary Biology, National Taiwan University, Taipei 10617, Taiwan

ABSTRACT

Microbes in the dark oceans are a key determinant of remineralization of sinking carbon particles. However, most marine ecosystem models overlook how microbes aggregate on particles and the microscale interactions between particle-associated microbes, making it difficult to obtain mechanistic insights on their vertical power-law decay pattern. Here, we present a spatial population model where the attachment and detachment processes of bacterial cells depend on local density of particle-associated bacteria. We show that the power-law relationship can emerge when the non-random aggregated distribution of bacteria is considered without any depth-specific environmental parameters. Furthermore, the comparison between model behavior and empirical patterns in the Pacific and Southern Ocean indicated that temperature-dependent hydrolysis rate and nutrient-dependent sinking rate of particles are key parameters to explain the regional variations of the power-law exponent. The mechanistic approach developed here provides a pathway to link micro-scale interactions between individuals to macro-scale food chain structures and carbon cycle.

1. Introduction

Over the last 20 years, the importance of microbial life in the dark oceans, one of the least explored biospheres, has been increasingly recognized. This interest exists because interactions between organic matter and microbes in the dark oceans are responsible for the remineralization of sinking particles (i.e., particulate organic carbon; POC) into carbon dioxide (CO₂), which has important consequences on global carbon cycle (Kwon et al., 2009; Ogawa et al., 2001). Dark ocean microbes (bacteria and their predators) can be characterized by how their abundance varied with depth (i.e., their vertical profiles from 100 to 200 m below sea surface down to the ocean floor), which has been approximated by a power-law decay function (Sohrin et al., 2010; Tanaka, 2009; Yang et al., 2014; Yokokawa et al., 2013). This pattern is comparable to the well-known power-law decay of POC sinking flux with depth (Berelson, 2012; Martin et al., 1987). Variation in the power-law exponent of POC flux, to which atmospheric pCO₂ is highly sensitive at a global scale (Kwon et al., 2009), has been previously attributed to ecological and physical processes (Berelson, 2012; Marsay et al., 2015; Nguyen et al., 2022 but also see Olli, 2015; Primeau et al., 2006). However, knowledge remains limited regarding: (1) the mechanisms driving the power-law decay pattern of microbes, and (2) how the

power-law exponents for microbial distribution vary regionally with environmental conditions. These limitations hinder our understanding of the mechanisms of POC remineralization and how microbial activity contribute to the variation in POC flux at a regional scale.

Evidence from profiles of bacterial activity (Nagata et al., 2000; Turley and Stutt, 2000; Yamada et al., 2012) and community genomics (Delong et al., 2006; Sunagawa et al., 2015), along with mathematical models (Miki et al., 2009), indicates that bacterial activity on the surface of sinking carbon particles is structured by depth. In addition, micro-scale studies have demonstrated the prevalence of the aggregated microbial distribution on the surface of particles (Azam and Malfatti, 2007; Stocker et al., 2008; Vadstein et al., 2012), and revealed both facilitative and repelling interactions between particle-associated and free-living bacteria (Grossart et al., 2003; Long and Azam, 2001). These lines of evidence challenge the traditional formulations of bacterial populations and consumer-resource dynamics in marine ecosystem models. In particular, past studies have overlooked bacterial activity on particles and assumed a simple Monod growth form in response to the concentration of organic carbon (Fasham et al., 1990; Laws et al., 2000), oversimplifying the interactions among particles, free-living bacteria, and particle-associated bacteria (Dunne et al., 2005; Laws et al., 2000; Miki, 2012; Miki et al., 2009; 2008; Miki and Yamamura, 2005).

* Corresponding author at: Faculty of Advanced Science and Technology, Ryukoku University, Otsu, Shiga 520-2194, Japan.

E-mail address: tkm.miki.ecology@gmail.com (T. Miki).

<https://doi.org/10.1016/j.jtbi.2024.111956>

Received 26 June 2024; Received in revised form 18 September 2024; Accepted 25 September 2024

Available online 29 September 2024

0022-5193/© 2024 Elsevier Ltd. All rights are reserved, including those for text and data mining, AI training, and similar technologies.

Recent models have focused on realistic aspects of particle characteristics while keeping the bacterial parameterization simple, as their aim is to quantitatively reproduce the power-law decay of POC flux. Key mechanisms include mixtures of particles with different degradation rate (Cael and Bisson, 2018) and depth-dependent factors such as sinking rate, degradation rate, and particle size spectrum (Omand et al., 2020). These mechanisms effectively reproduce the observed power-law decay in POC flux but do not focus on bacterial abundance distribution itself. Another line of recent models incorporates density-dependent growth of attached bacteria, detailed dynamics of extracellular enzyme, and depth-dependent environmental parameters. These models are able to quantitatively explain empirical patterns with a depth-independent sinking rate and a single type of particle (Mislan et al., 2014) or with reduction of particle size and sinking rate along degradation (Nguyen et al., 2022). Nevertheless, it should be noted that these models try to numerically explain the empirical bacterial abundance but do not focus on the power-law decay pattern itself.

However, it remains unclear whether microscale interactions between bacteria via chemotaxis (Stocker et al., 2008) and quorum sensing (Gram et al., 2002; Hmelo et al., 2011) are important only for bacterial survival and competition strategies or also for macroscale distribution of bacterial abundance and POC flux. To bridge the gap between recent advances in microscale studies and existing population dynamics models, this study proposes an alternative model for the power-law distribution that explicitly considers the microscale aggregated distribution of bacteria on particles.

Although we acknowledge that various environmental parameters are depth-dependent, e.g., temperature, water density, turbulent diffusion rate, and sinking rate of particles (Mislan et al., 2014; Nguyen et al., 2022; Omand et al., 2020) and that POC includes particles of various sizes (Cael and Bisson, 2018; Omand et al., 2020), our primary aim is to demonstrate that the macroscale power-law distribution can emerge from microscale density-dependent relationships between particles, free-living bacteria, and attached bacteria. These relationships autonomously change with depth, even when parameters are depth-independent and with a single, constant particle size. Since the focal mechanisms differ between models, our hypothesis and the findings from the recent models (Cael and Bisson, 2018; Mislan et al., 2014; Nguyen et al., 2022; Omand et al., 2020) are not mutually exclusive.

We also aim to link environmental parameters to model parameters and identify key determinants of the power-law exponent of bacterial abundance. This is done by comparing a statistical analysis of empirical data on vertical profiles of bacterial abundance and environmental parameters collected over a large spatial scale (i.e., the central Pacific Ocean and Southern Ocean, ranging from 67.5° S to 53.6° N) (Yang et al., 2010; Yokokawa et al., 2013) with a sensitivity analysis of model parameters.

To achieve these two aims, our spatial population model incorporated multiscale processes: particle state transitions at the microscale, driven by bacterial colonization to particles; demographic dynamics at the local scale (at each layer of the ocean), driven by particle hydrolysis and bacterial growth; and vertical distribution patterns at the macroscale, driven by diffusion and sinking.

2. Material and methods

2.1. Spatial population model

Model Framework—Below, we first describe the model variable settings that were used to capture the interactions between POC and bacteria. Then, the formulations were separately derived for: (1) the microscale interactions between bacteria and POC (fast processes), (2) the demographic processes of the bacterial population (slow process). The fast and slow processes were then incorporated into the equations that describe the temporal dynamics of bacteria and POC. Finally, vertical heterogeneity driven by sinking and mixing were incorporated to

form a one-dimensional spatial dynamic model.

Model Variables—We considered a bacterial population that have cells in two states: (1) free-living bacterial cells that are suspended in bulk water, and (2) particle-attached bacterial cells that form aggregates with carbon particles (POC). We developed a one-dimensional spatial population model with depth-specific total abundance of bacteria and POC, $B_T(z, t)$ cells/m³ and $A_T(z, t)$ particles/m³, respectively, at depth z meters and time t . This model differed from classical formulations (Hasumi and Nagata, 2014) and recent models (Mislan et al., 2014; Nguyen et al., 2022) in that it explicitly incorporates non-uniform distributions of particle-attached bacterial cells among particles at each depth by the abundance of particles, $A_n(z, t)$, which are colonized by n bacterial cells ($n = 0, 1, 2, \dots$) (Fig. 1a). The total abundance of particles and the total number of particle-attached bacteria are calculated as $A_T(z, t) = \sum_{n=0}^{+\infty} A_n(z, t)$, and $B_A(z, t) = \sum_{n=0}^{+\infty} nA_n(z, t)$, respectively. Total bacterial abundance $B_T(z, t)$ is the sum of B_A and free-living bacteria, $B_F(z, t)$ (Fig. 1b).

Microscale interactions between bacteria and POC—We assumed that the attachment rate of a single free-living bacteria to particles (A_n) and the detachment rate of a single particle-attached bacteria from A_n depend on local bacterial abundance (n); these two rates are presented as the function $a(n)$ and $d(n)$, respectively. Such a density-dependence process is not considered in other models (Kjørboe et al., 2002; Lambert et al., 2019). For each particle state ($n = 0, 1, 2, \dots$), we can describe the dynamics of the state transition as:

$$\frac{dA_n}{dt} = \underbrace{a(n-1)A_{n-1}B_F}_{\text{by attachment } A_{n-1} \rightarrow A_n} - \underbrace{a(n)A_nB_F}_{\text{by attachment } A_n \rightarrow A_{n+1}} + \underbrace{(n+1)d(n+1)A_{n+1}}_{\text{by detachment } A_{n+1} \rightarrow A_n} - \underbrace{nd(n)A_n}_{\text{by detachment } A_n \rightarrow A_{n-1}}. \quad (1)$$

The presence of bacteria on a particle either enhances or suppresses the further colonization of bacteria depending on strains (Grossart et al., 2003). The likely mechanisms for enhanced colonization include the attraction of free-living motile bacteria to dissolve organic matter (DOM) released from particles due to hydrolysis driven by the existing attached bacterial cells (Stocker et al., 2008), whereas the mechanism for suppressed colonization include the repelling of newer colonizers by antibiotics production (Long and Azam, 2001). Since the abundance and activity of particle-attached bacteria and particle hydrolysis rate are positively correlated (Middelboe et al., 1995), it is likely that DOM release from a particle and thus chemotactic activity of motile bacteria increases with the abundance of attached bacteria on the particle. In addition, quorum sensing, a cell-density-dependent signaling system, may affect the colonization process (Hmelo et al., 2011). Despite empirical evidence suggesting a positive relationship, the exact functional form between the local bacterial abundance already attached to a particle and the rate of subsequent attachment of free-living cells to the particle remains unclear. Therefore, we first derived the model equations with a general density-dependent function $a(n)$ and $d(n)$ (see also Miki & Yamamura 2005; Miki et al., 2008, 2009 for different formulations). Then, we used two specific formulations $a(n)$ for numerical calculations: linear density-dependence function $a_0 + a_1 n$ and the nonlinear density-dependence function $a_0 \exp(a_1 n)$, where a_0 and a_1 represent density-independent and dependent attachment coefficients, respectively. The linear and nonlinear formulations correspond to the case when no further interactions between attached bacterial cells on a particle are considered (the attractiveness via chemotaxis linearly increases with bacterial abundance only) and the case when a certain cooperative behavior is considered (Enke et al., 2018), respectively. Similarly, two examples $d_0 + d_1 n$ and $d_0 \exp(d_1 n)$ were considered for the detachment rate, which would be mediated by quorum sensing (Gram et al., 2002) or simply as the result of competition (Mislan et al., 2014). With $d_1 > 0$, our formulation corresponds to the case where negative

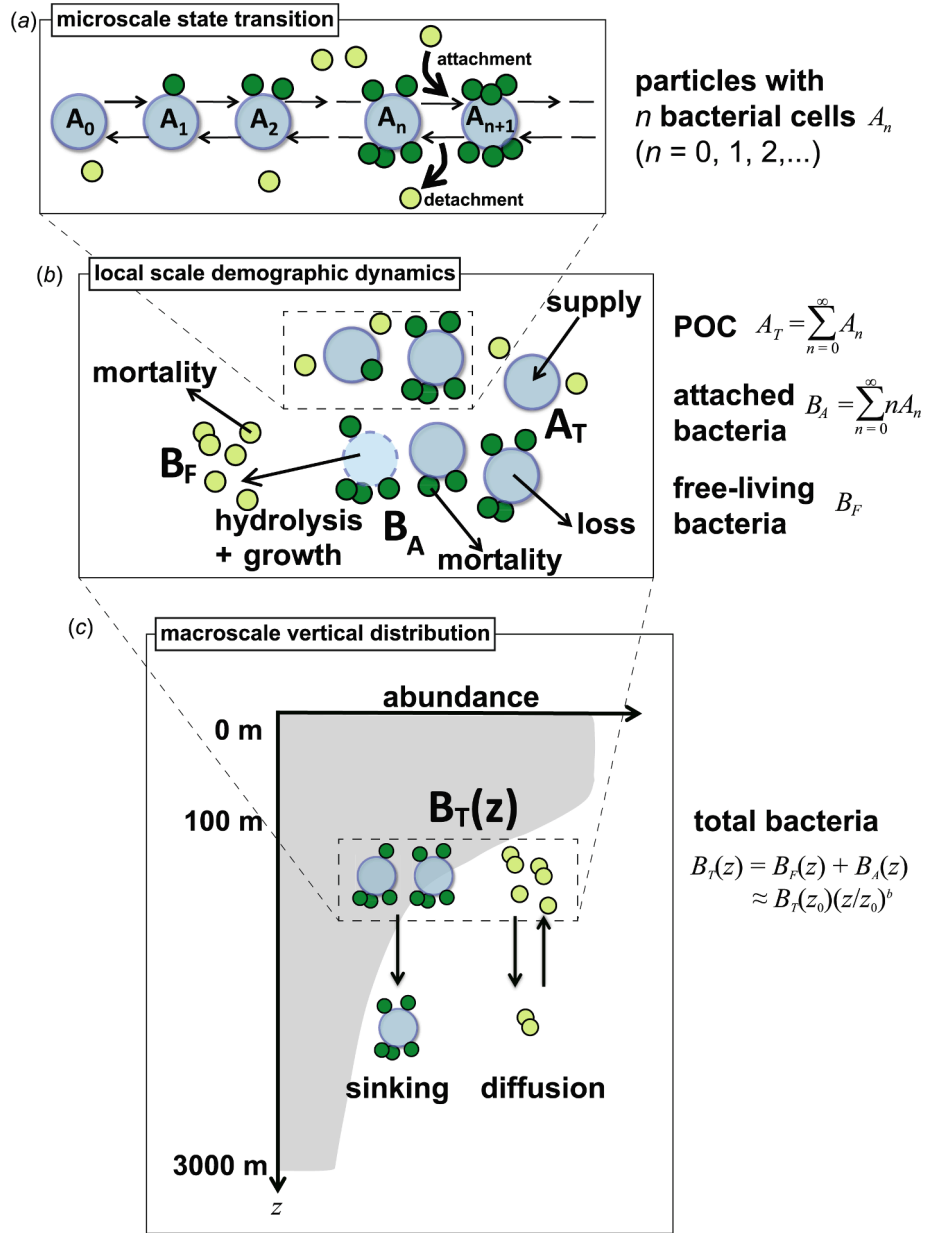


Fig. 1. Schematic diagrams illustrating the multiscale interactions between bacteria and particles. (a) Microscale state transition: shows particles, labeled A_n , with varying numbers ($n = 0, 1, 2, \dots$) of bacterial cells attached. The state of these particles changes with bacterial attachment to and detachment from them. (b) Local scale demographic dynamics: demonstrates how, at each depth, the number of particles is subject to change due to supply from primary production and losses from grazing and hydrolysis. Bacterial growth is driven by the consumption of hydrolyzed organic matter from particles, with mortality also influencing bacterial abundance. (c) Macroscale vertical distribution: illustrates the distribution of particles and bacteria throughout the water column. Turbulent diffusion results in their random movement upwards and downwards, while gravitational sinking specifically causes the downward movement of particles and attached bacteria. A successful model is expected to demonstrate a power-law decay with depth in total bacterial abundance, characterized by an exponent ($b < 0$). In our model setting, z_0 is the starting depth for regression, defined as the depth where maximum bacterial abundance occurred in depth ≥ 100 m.

interactions between attached bacterial cells enhance the detachment rate (see also Kjørboe et al., 2002 for density-independent detachment rate, corresponding to $d_1 = 0$ in our model, and Mislán et al., 2014 for density-dependent detachment rate).

We assumed that the attachment and detachment processes occur much faster than the demographic processes (Grossart et al., 2003; Lambert et al., 2019). This assumption allowed us to incorporate behavioral complexity of individual organisms into population models (Auger and Poggiale, 1996). Under this assumption, at each time t when the total abundance of bacteria (B_T) and that of particles (A_T) are given, the frequency of different states of particles ($P_n(z, t) = A_n(z, t)/A_T(z, t)$, $n = 0, 1, 2, \dots$) reaches equilibrium without the influence of demographic processes, as follows (setting $dA_n/dt = 0$ and also see Fig. 1a and Eqs. (A1) – (A4) in Appendix A):

$= 0, 1, 2, \dots$) reaches equilibrium without the influence of demographic processes, as follows (setting $dA_n/dt = 0$ and also see Fig. 1a and Eqs. (A1) – (A4) in Appendix A):

$$P_n = \frac{\lambda^n}{n!} P_0 \prod_{k=1}^n \frac{d_0 a(k-1)}{a_0 d(k)} \quad n \geq 1, \quad (2)$$

where $a_0 = a(0)$, $d_0 = d(0)$, $\lambda = (a_0/d_0)B_F$. Note that this distribution is identical to the Poisson distribution, with $P_0 = e^{-\lambda}$, when $a(n)$ and $d(n)$ are density-independent constants; importantly, it deviates from the Poisson distribution when $a(n)$ and $d(n)$ are density-dependent (Fig. S1).

With the specific linear ($a(n) = a_0 + a_1n$, $d(n) = d_0 + d_1n$) and exponential ($a(n) = a_0\exp(a_1n)$, $d(n) = d_0\exp(d_1n)$) density-dependent functions, Eq. (2) is reduced to the following, respectively,

$$P_n = P_0 \frac{\lambda^n}{n!} \prod_{k=1}^n \frac{1 + \left(\frac{a_1}{a_0}\right)(k-1)}{1 + \left(\frac{d_1}{d_0}\right)k} \quad n \geq 1, \tag{3}$$

and

$$P_n = P_0 \frac{\tilde{\lambda}(B_F)^n}{n!} \exp(-\alpha n^2) \quad n \geq 0, \tag{4}$$

where α in Eq. (4) represents the net density-dependent effect and is given as $\alpha = (d_1 - a_1)/2, \tilde{\lambda}(B_F) = (a_0/d_0)B_F \exp[-(a_1 + d_1)/2]$, and P_0 is a function of λ and α .

Demographic processes of bacteria and supply and hydrolysis processes of POC—We assumed that the free-living cells of bacteria are produced through the hydrolysis of particles (Fig. 1b). The hydrolysis rate of A_n is given by h_1n , i.e., it increases linearly with the local density n of bacteria attached to the particle (but see Enke et al., 2018; Mislan et al., 2014; Nguyen et al., 2022 for nonlinear formulation with interactions between attached bacteria). Two sources of mortality were assumed for bacteria: (1) loss of attached cells with the loss of the whole particle by the grazing of metazoan zooplankton, and (2) loss of free-living and attached cells by the grazing of protozoa, the rates of which are constant and given by m_A and m_B , respectively. We assumed that the abundance of POC increases with constant supply S_0 , and decreases with hydrolysis by attached bacteria and with grazing by metazoan zooplankton. The dynamics of particles are given by:

$$\begin{aligned} \frac{dA_T}{dt} &= \underbrace{S_0}_{\text{constant supply}} - \underbrace{\sum_{n=0}^{\infty} h_1 n A_n}_{\text{particle hydrolysis}} - \underbrace{m_A \sum_{n=0}^{\infty} A_n}_{\text{density independent loss due to metazoan zooplankt on grazing}} \\ &= S_0 - h_1 B_A - m_A A_T \equiv f_{A_T}. \end{aligned} \tag{5}$$

The total abundance of bacteria changes with time along the following dynamics:

$$\begin{aligned} \frac{dB_T}{dt} &= \underbrace{q_{POC} \cdot BGE / q_B \cdot \sum_{n=0}^{+\infty} h_1 n A_n}_{\text{production of free-living bacteria along particle hydrolysis}} - \underbrace{m_A \sum_{n=0}^{+\infty} n A_n}_{\text{loss of attached bacteria along with particle loss}} - \underbrace{m_B \left(\sum_{n=0}^{+\infty} n A_n + B_F \right)}_{\text{loss of bacteria due to grazing}} \\ &= (q_{POC} \cdot BGE / q_B h_1) B_A - m_A B_A - m_B (B_A + B_F) \equiv f_{B_T}, \end{aligned} \tag{6}$$

where q_{POC} , q_B , and BGE are the carbon biomass of a single particle, that of a single bacterial cell, and bacterial growth efficiency, respectively.

Incorporating microscale interactions and population growth—By combining the fast state distribution (Fig. 1a and Eq. (2)) and slow growth processes (Fig. 1b and Eqs. (5), (6)), we created the population dynamics model for local ecological processes (i.e., both microscale interactions and population growth) at each depth z . We assume that B_A and B_F are determined as the fast distribution when A_T and B_F are given. That is:

$$B_T = B_F + B_A(A_T, B_F). \tag{7}$$

However, it is not possible to write down B_F and B_A as the explicit function of B_T , so Eq. (6) cannot be closed with B_T . Therefore, we must convert Eq. (6) to the closed question of dB_F/dt by using the chain rule to Eq. (7):

$$\frac{dB_T}{dt} = \frac{dB_F}{dt} + \frac{\partial B_A}{\partial A_T} \frac{dA_T}{dt} + \frac{\partial B_A}{\partial B_F} \frac{dB_F}{dt}.$$

Then, using Eqs. (5) and (6), we obtain,

$$\frac{dB_F}{dt} = \left(1 + \frac{\partial B_A}{\partial B_F}\right)^{-1} \left(f_{B_T} - \frac{\partial B_A}{\partial A_T} f_{A_T}\right), \tag{8}$$

noting that $\frac{\partial B_A}{\partial B_F}$ is always positive (Eq.(A6)) and $\left(1 + \frac{\partial B_A}{\partial B_F}\right)^{-1}$ is well defined.

Using Eq. (8), Eqs. (5) and (6) are further converted into:

$$\frac{dA_T}{dt} = S_0 - \left(h_1 \frac{\theta_\infty}{1 + \psi_\infty} + m_A\right) A_T, \tag{9}$$

$$\begin{aligned} \frac{dB_F}{dt} &= \left(1 + \frac{\partial B_A}{\partial B_F}\right)^{-1} \\ &\times \left[\frac{\theta_\infty}{1 + \psi_\infty} \left\{ A_T \left(\frac{q_{POC}}{q_B} BGE \cdot h_1 - m_B + h_1 \frac{\theta_\infty}{1 + \psi_\infty} \right) - S_0 \right\} - m_B B_F \right], \end{aligned} \tag{10}$$

where θ_∞ , φ_∞ , ψ_∞ , and $\frac{\partial B_A}{\partial B_F}$ are given in Eqs. (A8) – (A10), and (A14). Although it would be counterintuitive for the hydrolysis rate in Eq. (5) to linearly increase with the abundance of attached bacteria (B_A) but remain independent of particle abundance, the hydrolysis responds linearly to A_T and nonlinearly to B_F (Eqn. (9)). In the special case of density-independent attachment and detachment, it is reduced to the well-known Michaelis-Menten type function (Eqn. (A20)).

Although we cannot explicitly derive the differential equation for B_T , we can calculate the total abundance of bacteria at any t , as $B_T(t) = B_F(t) + \frac{\theta_\infty}{1 + \psi_\infty} A_T(t)$. We regard these Eqs. (9) and (10) as the population dynamics without vertical spatial structure (non-spatial model). In other words, we interpret that these equations describe the local ecological processes occurring within each layer of the ocean.

Incorporating local processes and vertical physical processes—To study the vertical distribution of POC and bacterial abundance, we formulated a multi-layer model by coupling vertical physical processes (i.e., sinking and diffusion) (Fig. 1c) with local ecological processes. Specifically, we set depth-dependent supply rate of particles $S_0(z) > 0$ for $0 \leq z \leq 50$ m, and 0 for $z > 50$ m. Sinking and diffusion were the only sources of particle supply in the aphotic layers ($z > 50$ m). In the mixing layer ($0 \leq z \leq 50$ m), the diffusion rate was fast enough to homogenize the population distribution despite the depth-specific demographic processes. This is why we assumed a single layer only for the mixing layer. In deeper layers, the sinking rate is set as 10 m d^{-1} while diffusion rate is $1.0 \text{ cm}^2 \text{ s}^{-1}$. These are small enough to realize the spatially heterogeneous population distribution due to the depth-specific demographic processes.

For incorporating sinking and diffusion into local ecological processes, however, it is not possible to directly add these terms into Eqs. (9) and (10), because particles (A_T) and attached bacteria (B_A) sink but free-living bacteria (B_F) do not. To explicitly consider such differences between B_A and B_F , we need to start modifying Eqs. (5) and (6) as

$$\frac{\partial A_T(z, t)}{\partial t} = f_{A_T}(z, t) - s \frac{\partial A_T}{\partial z} + \frac{\partial}{\partial z} \left(D(z) \frac{\partial A_T}{\partial z} \right), \tag{11}$$

$$\frac{\partial B_T(z, t)}{\partial t} = f_{B_T}(z, t) - s \frac{\partial B_T}{\partial z} + \frac{\partial}{\partial z} \left(D(z) \frac{\partial B_T}{\partial z} \right), \tag{12}$$

where s is depth-independent sinking rate and $D(z)$ is depth-dependent turbulent diffusion rate (but depth-dependent in the surface layer ≤ 100 m depth only).

Following the derivation of Eqs. (9) and (10), our strategy to obtain the spatial population model with local processes was to first discretize Eqs. (11) and (12) into a set of ODEs (Eqs. (A15) and (A16) and then appropriately convert them into the spatially-discretized equations for

$A_T(z)$ and $B_F(z)$ (Eqs. (A18) and (A19)) using the chain rule (Eq. (A17); similar to Eq. (8)).

Notes on some assumptions— In order to keep the model analytically and numerically solvable while using biologically valid assumptions, some processes and parameters were not considered in the model. Since our primary focus is on the aphotic zone of the oceans and the population dynamics of heterotrophic bacteria, we did not explicitly consider the dynamics of phytoplankton in the surface oceans. Instead, their activity was parameterized as a fixed primary production, S_0 . Consequently, we did not account for the light spectrum and its variations with depth (see Heggerud et al., 2023). We neglected the bacterial replication and predation-induced mortality on each particle (Grossart et al., 2003; Kjørboe et al., 2003; Mislán et al., 2014; Nguyen et al., 2022), explicit hydrolysis of particles into dissolve organic carbon, and its consumption by free-living bacteria (Miki et al., 2009; Miki and Yamamura, 2005; Mislán et al., 2014). We did not explicitly consider microscale physical parameters that determine the encounter rate between particles and free-living bacteria, such as the diffusivity of randomly moving bacteria, the radius of bacteria and particles, and the Sherwood number (Kjørboe et al., 2002; Lambert et al., 2019; Mislán et al., 2014; Nguyen et al., 2022). Note that these parameters determine the density-independent attachment of bacteria in previous models, which corresponds to the parameter a_0 in our model framework. The chemotactic behavior that increases the encounter rate of bacteria to particles is modeled as an increase in ‘effective’ radius of particles (Lambert et al. 2019). Since we used a single and constant a_0 (and d_0) value, it implies that we neglected temporal changes in particles sizes due to gradual hydrolysis (Nguyen et al., 2022) as well as heterogeneity in particle sizes (i.e., size spectrum) (Omand et al., 2020).

2.2. Setting for model analysis

All of the numerical analyses and statistical analyses were conducted using C language and R4.3.1 (TeamCore, 2018), respectively. First, we evaluated the vertical distribution of POC flux ($=s \cdot A_T(z)$) and total bacterial abundance ($=B_F(z) + B_A(z)$) at the demographic equilibrium of our spatial population model, where s represented the depth-independent sinking rate of particles. In particular, we investigated how density-dependent interactions (i.e., $a_1 \neq 0$ or $d_1 \neq 0$) affect the emergence of power-law decay for both POC flux and total bacterial abundance. Numerical methods for solving the differential equations are described in the Supplementary Material (Appendix B. Numerical methods of approximation). The default parameter values for numerical calculations were summarized in Table S4.

To ensure efficient numerical calculations within a reasonable time frame (i.e., within 30 h, using a Xeon Silver 4108 1.80 GHz processor with 8 cores x 2), we first employed extremely small particle size (its carbon content is equivalent to 100 bacterial cells; Table S4) as the default parameter value. When choosing more realistic parameter values, which are represented by larger particle sizes equivalent to the carbon content of 10^6 bacterial cells, the production of free-living bacteria (B_F) from hydrolyzed particles and the value of λ become significantly larger (in Eqs. (3) and (4)). Under such scenario, numerical computation of the frequency distribution of particles (especially for P_0 in Eq. (A4)) requires truncating the infinite series at a specific upper limit (here set as 2λ). However, even with this truncation, computational time increases significantly with larger λ values. To address this challenge, we implemented an ‘offline’ approach (Walters, 1997) by pre-computing the relationship between λ and P_n , before conducting the simulation of the system’s time evolution, which is governed by differential equations that include the λ -dependent P_n function. Despite the necessity for approximating P_n as a normal distribution in this approach (Fig. S3), it significantly improves computational efficiency and streamlines the simulation process.

We fitted both the exponential model (i.e., $Y(z) \sim Y(z_0) \cdot \exp[b \cdot (z - z_0)]$) and the power-law model (i.e., $Y(z) \sim Y(z_0) \cdot (z/z_0)^b$) to the

equilibrium vertical distributions, in order to describe the pattern of decay in bacterial abundance and POC flux. Here, z_0 is the starting depth, defined as the depth where maximum bacterial abundance occurred in depths equal to or greater than 100 m. The coefficient b represented the exponential decay or power-law decay exponent. R^2 was calculated for both models. Although our model includes two depth-dependent parameters: $S_0(z)$ and $D(z)$, these are depth-independent in the aphotic zone ($z > 100$ m). Therefore, we aimed to reproduce the power-law distribution pattern without depth-dependent parameters.

Second, we examined the local sensitivity of the power-law decay exponent to various parameters (e.g., hydrolysis rate, bacteria growth efficiency, and sinking rate) in the spatial population model (see Appendix C. Sensitivity analysis). We also investigated how the power-law distribution changed with different model assumptions (i.e., variable sinking rate of particles and density-dependent bacterial mortality).

2.3. Statistical analysis of empirical data

To investigate empirical patterns, we obtained data on the vertical distribution of bacteria and environmental variables from the Full depth distribution of Microbial Abundance and Production (FddMAP) website (http://cesdweb.aori.u-tokyo.ac.jp/database/sites/FddMAP/FddMAP_EN.html) (Yang et al., 2010; Yokokawa et al., 2013). The number of data points at each station ranged from 23 and 37, we used the bacterial abundance at the depth ≥ 90 m and the maximum depth ranged from 1775 m to 5865 m. The stations ranged geographically from 67.5° S to 53.6° N. As with the spatial population model, we fitted both the exponential model and power-law model for each station to describe the decay in bacterial abundance ($Y(z)$) with increasing depth (z). Akaike information criterion (AIC) and R^2 were calculated for both the exponential and power-law models. Of note, the power-law model was better supported (i.e., lower AIC value and higher R^2 value) at all stations. For the environmental variables, we used the average value of either the whole water column or just the epipelagic zone (i.e., top 200 m). We used linear regression to elucidate the relationship between the fitted parameters (i.e., exponent b for the power-law model) and environmental variables.

2.4. Programming and analytical tools

We implemented the C programming language to numerically solve the spatial population model, which is a discretized reaction–diffusion–advection model, utilizing the 4th-order Runge-Kutta method with a fixed time interval. For statistical analysis and data visualization, we utilized R 4.2.1 (R core Team 2023). In addition, we used *Rmpfr* package (Maechler, 2023) to obtain high-precision numerical relationships between λ and P_n , as detailed in Appendix B.

3. Results

3.1. Modeled power law distribution of bacteria and POC flux

When density dependence in microscale particle-bacteria interactions was not considered ($a_1 = d_1 = 0$), total bacterial abundance decayed exponentially and went extinct at 1280 m ($< 1.0e-7$ cells m^{-3}) (Fig. 2b). The corresponding POC flux only followed power-law until 300 m depth (black line in Fig. 2a). In addition, we analytically showed that density independent particle-bacteria interactions led to a traditional Michaelis-Menten equation for the particle hydrolysis rate (Eq. (A20) in Appendix A). On the other hand, with the exponential density dependence of microscale interactions (Eq. (3)), both total bacterial abundance and POC flux followed power-law decay with depth until the modeled bottom layer (3000 m) (blue line in Fig. 2). Although there were slight differences in the exponent, the power-law relationship was maintained when linear density-dependent formulation (Eq.2) was used (Fig. S2) and when the density-dependent sinking rate and density-

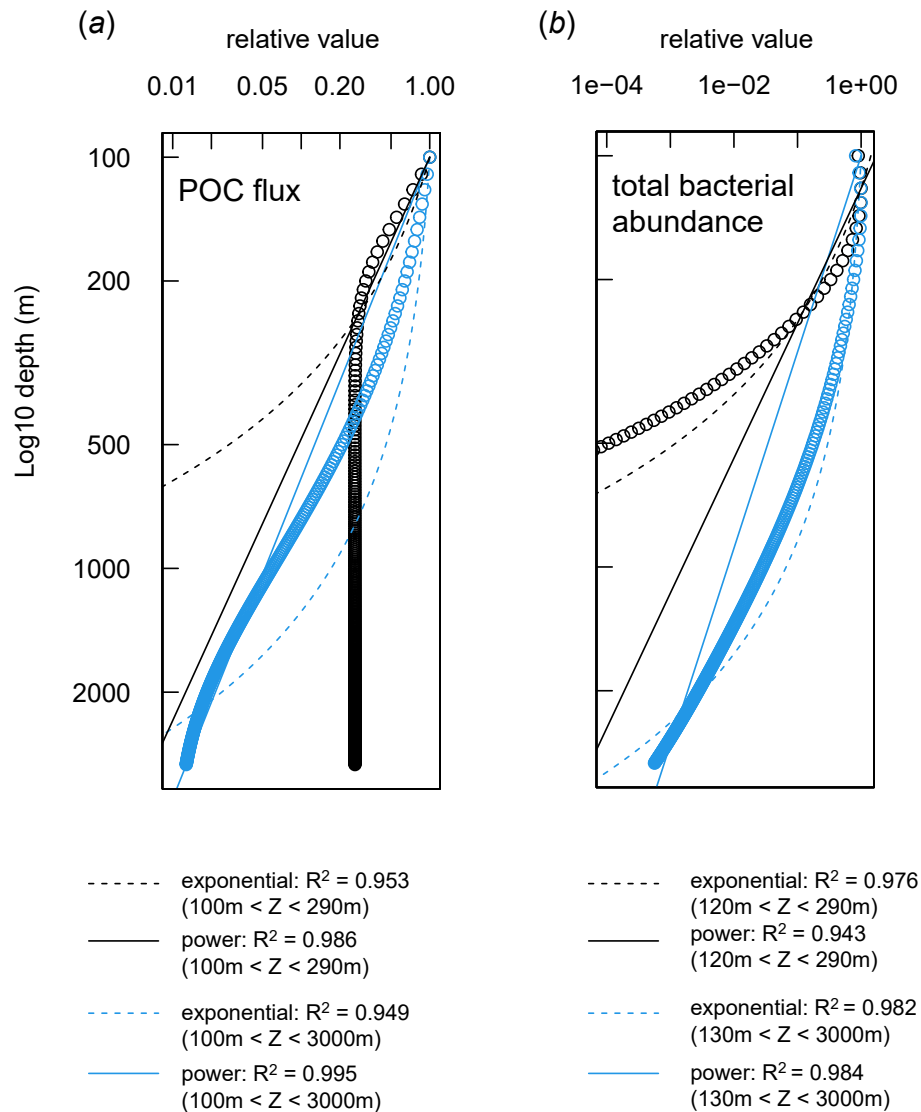


Fig. 2. Vertical distribution of POC flux (a) and total bacterial abundance (b) from the model. Circles represent the results obtained by numerically solving our spatial population model. With density-independent attachment and detachment processes (black lines), POC flux followed the power-law decay (solid black line), whereas total bacterial abundance followed exponential decay (dashed black line). With density-dependent processes (blue lines), both POC flux and total bacterial abundance followed power-law decay patterns (solid blue lines). Parameter values for the density-independent case are: $a_0 = 100 \text{ day}^{-1} [10^9 \text{ cells}]^{-1}$, $d_0 = 2000 \text{ cell}^{-1} \text{ day}^{-1}$, $a_1 = d_1 = 0 [10^9 \text{ cells}]^{-1}$, and $m_B = 0.02 \text{ day}^{-1}$. In comparison, parameter values for the density-dependent case were default values (Table S4). The horizontal axis depicts the relative value, which is standardized by the maximum value recorded in the region $\geq 100 \text{ m}$ depth. The starting depth for these regressions was also the depth at which the maximum value was recorded. Both of the horizontal and vertical axes are \log_{10} scaled. The maximum depth was set as 3010 m (Table S4). The ranges of the depth (z) for which exponential regression and power-law regression were conducted are shown below each panel of the graph. For the density-dependent case, the power-law exponents for POC flux and total bacterial abundance were -1.460 and -2.093 , respectively.

dependent bacterial mortality were considered along with the exponential density-dependent attachment/detachment (Table S1). By incorporating more realistic parameter values and employing a normal distribution approximation (Fig. S3), we achieved significantly more numerically-accurate slopes for the total bacterial abundance (-1.673 and -1.818 for the linear and exponential density dependence models, respectively, as shown in Fig. S4). However, in order to emphasize theoretical aspects over specific numerical values, the subsequent results from our model are presented based on the exponential density-dependent formulation without the normal distribution approximation (Eq. (4)) and using the default parameter set (Table S4).

3.2. Empirical patterns from the central Pacific and Southern Ocean

The maximum bacterial abundance ($\geq 90 \text{ m}$ depth) ranged from

1.359 to $8.399 [10^5 \text{ cells mL}^{-1}]$, while at the bottom it ranged from 0.083 to $0.418 [10^5 \text{ cells mL}^{-1}]$. The empirical distribution of total bacterial abundance also showed power-law decay. The power-law exponent showed regional variations from 67.5° S to 53.6° N , with values ranging from -1.2674 (steepest) to -0.4751 (shallowest) (Fig. 3). By fitting linear models between the power-law exponent and the environmental variables, we showed that the exponent was negatively correlated with temperature (Fig. 3, Fig. 4a). Moreover, the decay in bacterial abundance was faster (more negative exponent) when salinity was higher (Fig. 4b). However, it was slower (less negative exponent) with other parameters, including a higher potential density of seawater (Fig. 4c), more dissolved oxygen (DO; Fig. 4d), higher nutrient levels (NO_3^- , Si, and PO_4^{3-} ; Fig. 4f, h, i), and higher Chlorophyll-a (chl.a; Fig. 4j), when the whole water column averaged environmental values were used (Fig. 4 and Table S2; also see Fig. S5 for the epipelagic zone [i.

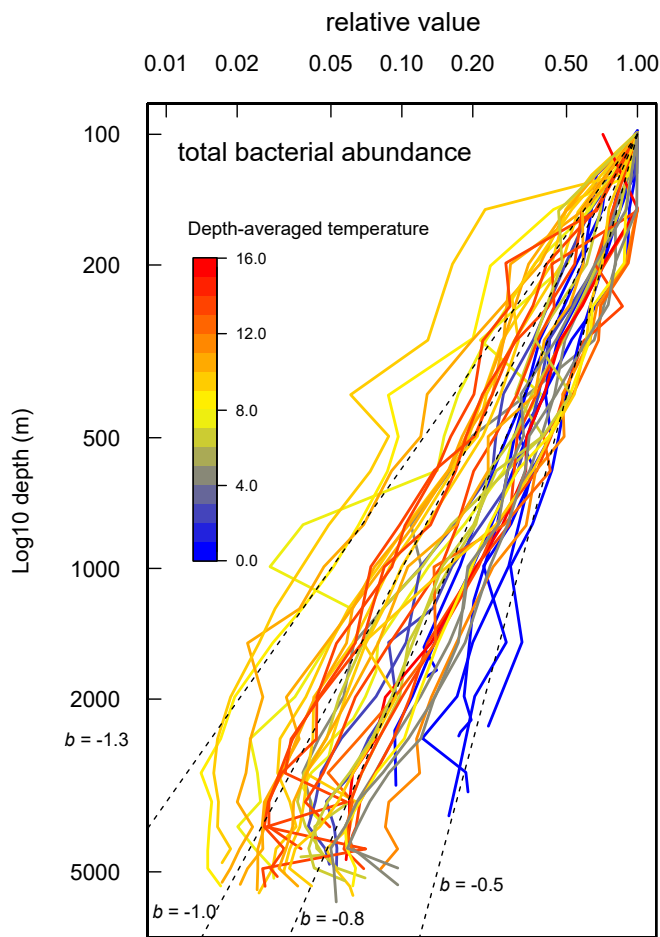


Fig. 3. Regional variation in the vertical distribution of total bacterial abundance from the Pacific Ocean and Southern Ocean. Dashed lines represent the power-law decay function, $B(z) = B(100)(z/100)^b$, with different exponents of b ($-1.3 \sim -0.5$), where B and z represent the total abundance of bacteria and depth, respectively. The color of each line represents the depth-averaged temperature value.

e., top 200 m] averages). There was no significant relationship between the exponent and apparent oxygen utilization (AOU), bacterial production, and viral abundance (Fig. 4e, k, l). The slope coefficients from the standardized linear regression represent empirical environmental sensitivity (i.e., the degree of the dependence of the power-law exponent on environmental variables) and are summarized in Fig. 5a.

3.3. Model sensitivity and comparison to empirical patterns

To compare empirical environmental sensitivity (Fig. 5a) and model behavior, we evaluated the sensitivity of the model parameters (Fig. 5b). We found that the exponent of bacterial abundance was more sensitive than that of POC for the four major parameters (d_1 , a_1 , h_1 , and s) (Appendix C, Table S3). Focusing on the model parameter sensitivity for the exponent of bacterial abundance, we found that greater density-dependent detachment rate (d_1), greater sinking rate (s), smaller density-dependent attachment rate (a_1), smaller hydrolysis rate (h_1), and smaller bacterial growth efficiency (BGE) produced less negative exponent (slower decay). In comparison, all other parameters (a_0 , d_0 , S_0 , and m_B) had only minor effects (Fig. 5b).

4. Discussion

The current study demonstrated that density-dependent microscale interactions between bacteria and sinking particles (Hmelo et al., 2011;

Urvoy et al., 2022) potentially represent a new mechanism by which the macroscale vertical distribution of bacteria emerges in the ocean. In particular, density-dependent attachment to and detachment from sinking particles can be key processes for qualitatively reproducing the empirical power-law decay patterns of bacterial abundance. In comparison, density-independent processes resulted in unrealistic exponential decay of bacterial abundance, if depth-dependency of environmental parameters and degradation rate were not considered as other models (Mislán et al., 2014; Nguyen et al., 2022; Omand et al., 2020). Further numerical calculations indicated that the power-law exponent was highly sensitive to density-dependent attachment and detachment processes. In addition, the presence of power-law decay was robust, even when relaxing part of the model assumptions (i.e., the constant sinking rate of particles and density-independent mortality of bacteria) (Table S1). For example, when negative density-dependent sinking rate was considered ($\beta = -0.01$, Table S1), we obtained the biologically reasonable response that POC flux and bacterial abundance decays with steeper slopes, as the consequence of slower sinking rate than the default setting.

Empirical patterns showed that power-law decay was ubiquitously present from 67.5° S to 53.6° N of the central Pacific Ocean and Southern Ocean, and that the decay exponents varied with environmental factors. Greater temperature generated steeper, more negative exponents, which corresponded to the modeled effect of the greater decomposition rate of particles (i.e., greater hydrolysis rate h_1). Similarly, greater silicate, Chlorophyll-a (proxy of primary production), and nutrient status generated less negative exponents, which could be explained by a higher sinking rate of particles in the model. Former environmental conditions might have favored the dominance of large-celled species in the phytoplankton community (Dunne et al., 2005), resulting in higher average sinking rates of organic matter produced by phytoplankton communities.

We applied a powerful theoretical technique from population biology (namely, time scale separation; Auger et al., 2008; Cordoleani et al., 2013; Cosner et al., 1999) to microbial oceanography, advancing our current understanding of the macroscopic spatial patterns of bacterial assemblages. To avoid computation-intensive agent-based simulation models, we assumed that attachment and detachment processes occurred much faster than demographic processes. This assumption is ecologically reasonable, because the attachment and detachment of bacteria occur at scales of minutes to hours (i.e., ‘fast distribution’) (Kjørboe et al., 2002). In comparison, replication and mortality occur at a scale of days (i.e., ‘slow growth’, but see Kjørboe et al. 2003; Enke et al. 2019). Our model described the dynamics of macroscopic variables (i.e., abundance of particles and bacteria) without needing to simulate detailed individual-level dynamics. This type of simple differential equation framework is necessary when incorporating the detailed ecology of microbes into the already-complicated ocean circulation models (Hasumi and Nagata, 2014).

Furthermore, we showed that the density-dependent attachment and detachment of bacteria predicts a weighted Poisson distribution (WPD, Eq. (4), which is under-dispersed relative to the Poisson distribution; Fig. S1). To represent over- and under-dispersion, various WPD have been proposed, such as two-parameter exponentially-weighted Poisson (EWP) (Sellers et al., 2012). Here, we derived another EWP with the novel weight function $\exp(-\alpha n^2)$ (Yoneya et al., 2021). Deviation from Poisson could be evaluated with a Chi-squared test. Also, the goodness of fit for the new EWP (two parameters, λ , and α) could be compared against that of the Poisson distribution. Testing whether the empirical distribution of bacteria is under-dispersed provides information on the microscale non-random interactions between sinking particles and bacteria. Also, these tests could be naturally extended to detect non-random interactions between bacteria and their predators in microbial food chains developed on sinking particles (Seymour et al., 2009; Tanaka, 2009).

There are still inconsistent results regarding the existence of density-

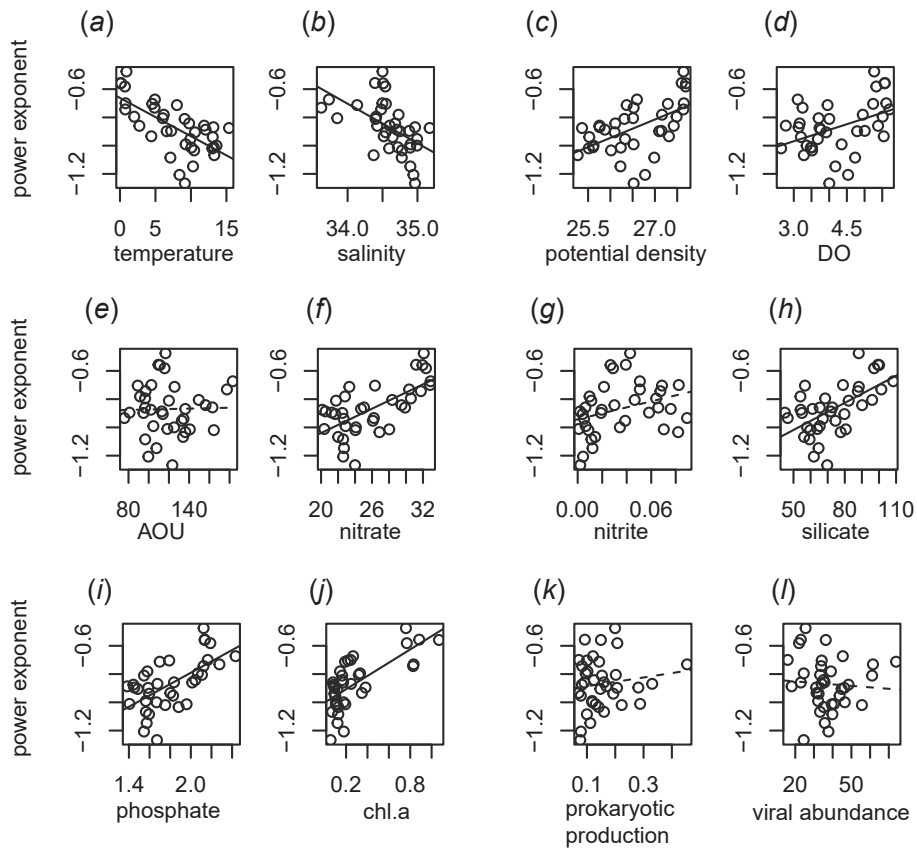


Fig. 4. Relationship between the power-law exponent and whole-depth averaged environmental parameter values. Dashed lines represent a non-significant slope from a linear regression ($P \geq 0.05$).

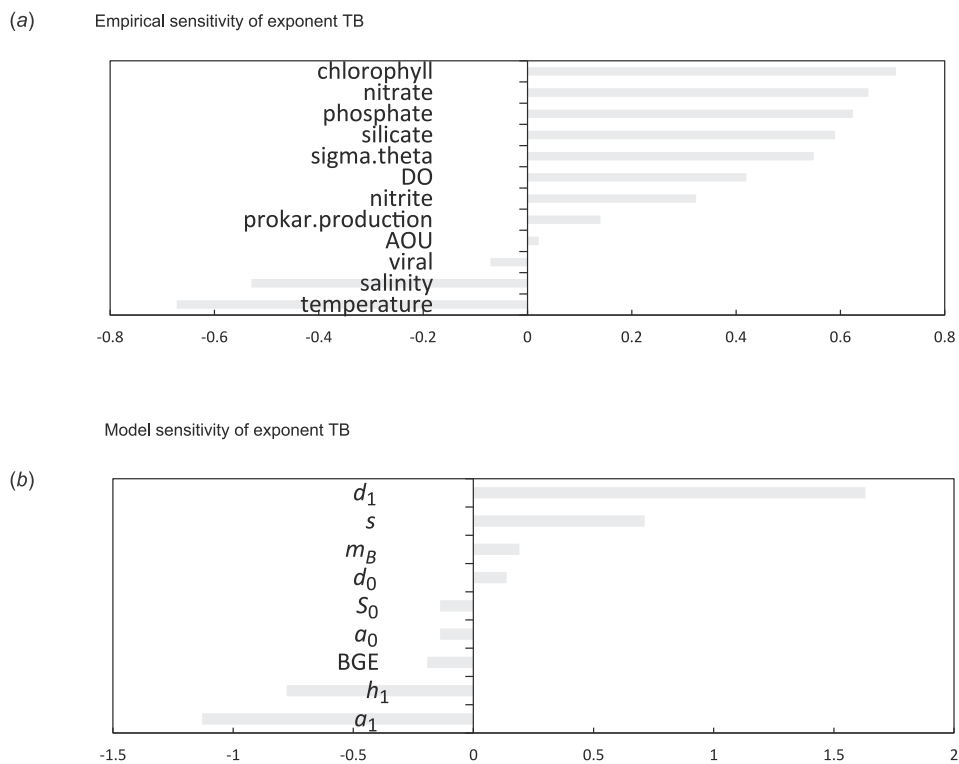


Fig. 5. Empirical environmental sensitivity (a) and model parameter sensitivity (b). Model parameter sensitivity regarding the power-law exponent was calculated based on the methods shown in Supplementary Material (Appendix C, ‘Sensitivity Analysis’). Empirical environmental sensitivity represents the slope coefficient from the standardized linear regression, with whole-depth averaged environmental parameter values.

dependency in attachment and detachment processes. Recent studies showed that models with density-independent attachment can well explain the hydrolysis rate of particles (Enke et al., 2018), and early colonization patterns of various taxa also imply the passive attachment of bacterial cells (Datta et al., 2016). At the same time, other studies demonstrated the effect of early colonizers on the attachment and growth of subsequent colonizers (Grossart et al., 2003), or suggested chemotactic behavior of some colonizers (Datta et al., 2016; Stocker et al., 2008). The common limitation in these empirical approaches is that it is difficult to clearly distinguish the effect of attachment, local population growth, and detachment from each other by using the time series of total abundance or community composition of attached bacteria (Kjørboe et al., 2002). However, as one of the advantages, our model derivation suggests that independent parameter values regarding attachment and detachment are not necessary for reproducing the qualitative pattern. Instead, we only need the ratio of density-independent attachment and detachment rate (a_0/d_0) and the net effect of density-dependence (a_1-d_1) for the exponential density-dependent formulations (Eq. (4)).

Our model qualitatively reproduced the power-law decay of POC flux but with a novel mechanism different from other models (Cael and Bisson, 2018; Mislan et al., 2014; Nguyen et al., 2022; Omand et al., 2020). In past theoretical attempts, the mechanism underlying the power-law decay in POC flux include depth-dependent sinking rate, detailed dynamics of exoenzymes (Mislán et al., 2014; Nguyen et al., 2022), density-dependent bacterial growth (Nguyen et al., 2022), depth-dependent particle degradation rate, and size spectrum of particles (Omand et al., 2020) or mixture of particles with different degradation rates (Cael and Bisson, 2018). Our model used a depth-independent sinking rate and a single and constant particle size with much simpler formulations for hydrolysis and physical environments than the models above (Mislán et al., 2014; Nguyen et al., 2022). Even with such simple settings, the non-Poisson distribution of attached bacterial cells at microscale, which has never been considered in other models, generates a depth-dependency of particle degradation rate and result in the power-law decay patterns of POC flux and bacteria abundance. Our model therefore provides an alternative mechanism for the power-law patterns but this mechanism and the existing mechanisms above are not mutually exclusive.

Focusing on the vertical distribution of total bacterial abundance, we overlooked any interspecific variation in the ecological parameters within a highly diverse bacterial community and regarded it as a homogeneous population. However, other studies, including our previous model, examined biodiversity (Boeuf et al., 2019; Mestre et al., 2018; Miki et al., 2008; Tréguer et al., 2018) and environmental gene networks (Guidi et al., 2016) as the determinants of microbe-mediated sinking flux of carbon. We note that the proposed microscale density-dependent interactions are not mutually exclusive to these recently emerging hypotheses. The effects of biodiversity and gene network might additively act on the flux of sinking particles, or these effects could be indirect, through influences on non-random interactions between bacterial individuals (Cordero and Datta, 2016).

Our model has shown promising results in predicting power-law exponents that align quantitatively with empirical observations. The power-law exponent for POC flux from the model (ranging from $-1.5 \sim -0.8$, Fig. 2 and Fig. S2) closely corresponds to well-established empirical ranges ($-1.3 \sim -0.6$, Berelson 2012). However, a discrepancy arises when examining the predicted exponent for bacterial abundance under default parameter values ($-2.7 \sim -2.0$, Fig. 2 and Fig. S2), which is considerably steeper than empirical values ($-1.3 \sim -0.55$, Sohrin et al., 2010; Tanaka, 2009). This gap has been effectively addressed by incorporating more realistic particle sizes and adopting an offline approach to handle a large number of attached bacteria per particle (in the order of 10^3 , see [2.6] of `depth_model_fit.nb.html`). This setting realized a considerably shallower slope ($-1.8 \sim -1.7$, Fig. S4), aligning more closely with the empirical values. Importantly, this

suggests that the existing quantitative gap can be significantly reduced through improved parameter choices. Nevertheless, it is critical to acknowledge two overlooked features in our model. Firstly, we assumed that newly-produced bacterial cells on particles are immediately released into the surrounding water along with hydrolysis loss of particles, overlooking the actual scenario where bacterial cells replicate and persist on the particle. Incorporating this consideration could result in a more accurate representation of attached bacterial abundance, on the order of 10^5 – 10^6 (Kjørboe et al., 2003; 2002), and significantly contribute to density-dependent population growth (Datta et al., 2016). Secondly, the exclusion of factors such as bacterial growth with non-sinking particles, dissolved organic carbon (DOC), and autotrophy (Herndl and Reinthaler, 2014; Miki et al., 2008; Miki and Yamamura, 2005) would underestimate bacterial growth rate. Including these factors is likely to lead to a shallower exponent of bacterial decay, making the prediction closer to the empirical values. To address these issues in an analytically-tractable modeling framework, future studies need to use different mathematical approaches (e.g., integral projection models, Rees et al., 2014).

Our framework, which links microscale interactions to macroscale patterns, represents a promising and evolving approach to modeling aquatic ecosystems (Wickman et al., 2024). Specifically, a microscopic perspective highlights that the interactions between resources and microbes are patchily distributed (Azam and Malfatti, 2007) despite being diluted under bulk concentration, therefore being mischaracterized by spatially homogeneous models. One possible model extension would be the explicit consideration of bacterial mortality agents (e.g., protozoa and their non-random behavior, Seymour et al., 2008). Another direction would be the inclusion of non-random variation of bacterial diversity on particles, depending on particle size (Mestre et al., 2017a,b). These extensions could help advance our understanding on how microscale interactions influence the spatial distribution of bacterial communities at the macroscale, and thus carbon remineralization processes in the deep oceans.

Declaration of Generative AI and AI-assisted technologies in the writing process

During the preparation of this work the authors used ChatGPT 4o in order to improve language and readability. After using this tool/service, the authors reviewed and edited the content as needed and take full responsibility for the content of the publication.

CRedit authorship contribution statement

Takeshi Miki: Writing – review & editing, Writing – original draft, Visualization, Methodology, Formal analysis, Conceptualization. **Po-Ju Ke:** Writing – review & editing, Writing – original draft, Visualization, Formal analysis.

Declaration of competing interest

The authors declare that they have no known competing financial interests or personal relationships that could have appeared to influence the work reported in this paper.

Data availability

No data were collected for this study. Programming codes are available at https://github.com/tksmiki/power_bac.

Acknowledgment

This work was supported by Ministry of Science and Technology (MOST, Taiwan) (NSC100-611-M-00-010) and Grant-in-Aid for Scientific Research (19H05667, 19H00956 and 23H00538) of JSPS (to TM).

PJK is supported by the Taiwan Ministry of Education Yushan Fellow Program (MOE-110-YSFAG-0003-001-P1) and Taiwan National Science and Technology Council (MOST 111-2621-B-002-001-MY3).

Supplementary material

Supplementary material to this article can be found online at <https://doi.org/10.1016/j.jtbi.2024.111956>.

References

- Auger, P., de La Parra, R.B., Poggiale, J.C., Sánchez, E., Sanz, L., 2008. Aggregation methods in dynamical systems and applications in population and community dynamics. *Phys. Life Rev.* 5, 79–105. <https://doi.org/10.1016/j.plev.2008.02.001>.
- Auger, P., Poggiale, J.C., 1996. Emergence of population growth models: fast migration and slow growth. *J. Theor. Biol.* 182, 99–108.
- Azam, F., Malfatti, F., 2007. Microbial structuring of marine ecosystems. *Nat. Rev. Microbiol.* 5, 782–791. <https://doi.org/10.1038/nrmicro1747>.
- Berelson, W., 2012. The flux of particulate organic carbon into the ocean interior: a comparison of four U.S. JGOFS regional studies. *Oceanography*. <https://doi.org/10.5670/oceanog.2001.07>.
- Boeuf, D., Edwards, B.R., Eppley, J.M., Hu, S.K., Poff, K.E., Romano, A.E., Caron, D.A., Karl, D.M., DeLong, E.F., 2019. Biological composition and microbial dynamics of sinking particulate organic matter at abyssal depths in the oligotrophic open ocean. *Proc. Natl. Acad. Sci.* <https://doi.org/10.1073/pnas.1903080116>, 201903080.
- Cael, B.B., Bisson, K., 2018. Particle flux parameterizations: quantitative and mechanistic similarities and differences. *Front. Mar. Sci.* 5, 395. <https://doi.org/10.3389/fmars.2018.00395>.
- Cordero, O.X., Datta, M.S., 2016. Microbial interactions and community assembly at microscale. *Curr. Opin. Microbiol.* 31, 227–234. <https://doi.org/10.1016/j.mib.2016.03.015>.
- Cordoleani, F., Nerini, D., Morozov, A., Gauduchon, M., Poggiale, J., 2013. Scaling up the predator functional response in heterogeneous environment: when holling type III can emerge? *J. Theor. Biol.* 336, 200–208. <https://doi.org/10.1016/j.jtbi.2013.07.011>.
- Cosner, C., DeAngelis, D.L., Ault, J.S., Olson, D.B., 1999. Effects of spatial grouping on the functional response of predators. *Theor. Popul. Biol.* 56, 65–75.
- Datta, M.S., Sliwerska, E., Gore, J., Polz, M.F., Cordero, O.X., 2016. Microbial interactions lead to rapid micro-scale successions on model marine particles. *Nat. Commun.* 7. <https://doi.org/10.1038/ncomms11965>.
- Delong, E.F., Preston, C.M., Mincer, T., Rich, V., Hallam, S.J., Frigaard, N., Martinez, A., Sullivan, M.B., Edwards, R., Brito, B.R., Chisholm, S.W., Karl, D.M., 2006. Community Genomics among microbial assemblages in the Ocean's Interior. *Science* 311, 496–503. <https://doi.org/10.1126/science.1120250>.
- Dunne, J.P., Armstrong, R.A., Gnanadesikan, A., Sarmiento, J.L., 2005. Empirical and mechanistic models for the particle export ratio. *Global Biogeochem. Cycles* 19, 1–16. <https://doi.org/10.1029/2004GB002390>.
- Enke, T.N., Datta, M.S., Schwartzman, J., Barrere, J., Pascual-garci, A., Cordero, O.X., Pascual-garci, A., 2019. Modular Assembly of Polysaccharide-Degrading Marine Microbial Communities Report Modular Assembly of Polysaccharide-Degrading Marine Microbial Communities 1528–1535. <https://doi.org/10.1016/j.cub.2019.03.047>.
- Enke, T.N., Leventhal, G.E., Metzger, M., Saavedra, J.T., Cordero, O.X., 2018. Microscale ecology regulates particulate organic matter turnover in model marine microbial communities. *Nat. Commun.* 9. <https://doi.org/10.1038/s41467-018-05159-8>.
- Fasham, M., Ducklow, H., McKelvie, S., 1990. A nitrogen-based model of plankton dynamics in the oceanic mixed layer. *J. Mar. Res.* 48, 591–639.
- Gram, L., Grossart, H.P., Schlingloff, A., Kjørboe, T., 2002. Possible quorum sensing in marine snow bacteria: production of acylated homoserine lactones by Roseobacter strains isolated from marine snow. *Appl. Environ. Microbiol.* 68, 4111–4116. <https://doi.org/10.1128/AEM.68.8.4111-4116.2002>.
- Grossart, H.P., Kjørboe, T., Tang, K., Ploug, H., 2003. Bacterial colonization of particles: growth and interactions. *Appl. Environ. Microbiol.* 69, 3500. <https://doi.org/10.1128/AEM.69.6.3500>.
- Guidi, L., Chaffron, S., Bittner, L., Eveillard, D., Larhimi, A., Roux, S., Darzi, Y., Audic, S., Berline, L., Brum, J.R., Coelho, L.P., Cesar, J., Espinoza, I., Malviya, S., Sunagawa, S., Dimier, C., Kandels-lewis, S., Picheral, M., Poulain, J., 2016. Plankton networks driving carbon export in the oligotrophic ocean. *Nature* 532, 465–470. <https://doi.org/10.1038/nature16942>.
- Hasumi, H., Nagata, T., 2014. Modeling the global cycle of marine dissolved organic matter and its influence on marine productivity. *Ecol. Model.* 288, 9–24. <https://doi.org/10.1016/j.ecolmodel.2014.05.009>.
- Heggerud, C.M., Lam, K.-Y., Wang, H., 2023. Niche differentiation in the light spectrum promotes coexistence of phytoplankton species: a spatial modelling approach. *J. Math. Biol.* 86, 54. <https://doi.org/10.1007/s00285-023-01890-z>.
- Herdnd, G.J., Reinthaler, T., 2014. Europe PMC Funders Group Microbial control of the dark end of the biological pump 6, 718–724. <https://doi.org/10.1038/ngeo1921>.
- Hmelo, L.R., Mincer, T.J., Van Mooy, B.a.S., 2011. Possible influence of bacterial quorum sensing on the hydrolysis of sinking particulate organic carbon in marine environments. *Environ. Microbiol. Rep.* 3. <https://doi.org/10.1111/j.1758-2229.2011.00281.x>.
- Kjørboe, T., Tang, K., Grossart, H., Ploug, H., 2003. Dynamics of Microbial Communities on Marine Snow Aggregates: Colonization, Growth, Detachment, and Grazing Mortality of Attached Bacteria 69, 3036–3047. <https://doi.org/10.1128/AEM.69.6.3036>.
- Kjørboe, T., Grossart, H.P., Ploug, H., Tang, K., 2002. Mechanisms and rates of bacterial colonization of sinking aggregates. *Appl. Environ. Microbiol.* 68, 3996. <https://doi.org/10.1128/AEM.68.8.3996>.
- Kwon, E.Y., Primeau, F., Sarmiento, J.L., 2009. The impact of remineralization depth on the air–sea carbon balance. *Nat. Geosci.* 2, 630–635. <https://doi.org/10.1038/ngeo612>.
- Lambert, B.S., Fernandez, V.I., Stocker, R., 2019. Motility drives bacterial encounter with particles responsible for carbon export throughout the ocean. *Limnol. Oceanogr.* Lett. 4, 113–118. <https://doi.org/10.1002/lo12.10113>.
- Laws, E.E.A., Falkowski, P.P.G., Smith, W., Ducklow, H., McCarthy, J.J.J., Smith Jr, W. O., Ducklow, H., McCarthy, J.J.J., 2000. Temperature effects on export production in the open ocean. *Global Biogeochem. Cycles* 14, 1231–1246. <https://doi.org/10.1029/1999GB001229>.
- Long, R.A., Azam, F., 2001. Antagonistic interactions among marine pelagic bacteria. *Appl. Environ. Microbiol.* 67, 4975. <https://doi.org/10.1128/AEM.67.11.4975>.
- Maechler, M., 2023. Rmpfr: R MPFR - Multiple Precision Floating-Point Reliable. R package version 0.9-1.
- Marsay, C.M., Sanders, R.J., Henson, S.A., Pabortsava, K., Achterberg, E.P., Lampitt, R.S., 2015. Attenuation of sinking particulate organic carbon flux through the mesopelagic ocean. *Proc. Natl. Acad. Sci.* 112, 1089–1094. <https://doi.org/10.1073/pnas.1415311112>.
- Martin, J., GA, K., DM, K., Broenkow, W., 1987. VERTEX: carbon cycling in the northeast Pacific. *Deep-Sea Research* 34, 267–285.
- Mestre, M., Borrull, E., Sala, M., Gasol, J.M., 2017a. Patterns of bacterial diversity in the marine planktonic particulate matter continuum. *ISME J.* 11, 999–1010. <https://doi.org/10.1038/ismej.2016.166>.
- Mestre, M., Ferrera, I., Borrull, E., Ortega-Retuerta, E., Mbedi, S., Grossart, H.P., Gasol, J. M., Sala, M.M., 2017b. Spatial variability of marine bacterial and archaeal communities along the particulate matter continuum. *Mol. Ecol.* 26, 6827–6840. <https://doi.org/10.1111/mec.14421>.
- Mestre, M., Ruiz-González, C., Logares, R., Duarte, C.M., Gasol, J.M., Sala, M.M., 2018. Sinking particles promote vertical connectivity in the ocean microbiome. *Proc. Natl. Acad. Sci. USA* 115, E6799–E6807. <https://doi.org/10.1073/pnas.1802470115>.
- Middelboe, M., Søndergaard, M., Letarte, Y., Borch, N., 1995. Attached and free-living bacteria: production and polymer hydrolysis during a diatom bloom. *Microb. Ecol.* 29, 231–248.
- Miki, T., 2012. Bacterial community should be considered in ecosystem model in the ocean?—Comparison between community-based model, black box model, and exponential decay model. *Interdiscip. Stud. Environ. Chem. – Environ. Pollut. Ecotoxicol.* 407–418.
- Miki, T., Giuggioli, L., Kobayashi, Y., Nagata, T., Levin, S.a., 2009. Vertically structured prokaryotic community can control the efficiency of the biological pump in the oceans. *Theor. Ecol.* 2, 199–216. <https://doi.org/10.1007/s12080-009-0042-8>.
- Miki, T., Yamamura, N., 2005. Theoretical model of interactions between particle-associated and free-living bacteria to predict functional composition and succession in bacterial communities. *Aquat. Microb. Ecol.* 39, 35–46. <https://doi.org/10.3354/ame039035>.
- Miki, T., Yokokawa, T., Nagata, T., Yamamura, N., 2008. Immigration of prokaryotes to local environments enhances remineralization efficiency of sinking particles: a metacomunity model. *Mar. Ecol. Prog. Ser.* 366, 1–14. <https://doi.org/10.3354/meps07597>.
- Mislan, K.A.S., Stock, C.A., Dunne, J.P., Sarmiento, J.L., 2014. Group behavior among model bacteria influences particulate carbon remineralization depths. *J. Mar. Res.* 72, 183–218. <https://doi.org/10.1357/002224014814901985>.
- Nagata, T., Fukuda, H., Fukuda, R., Koike, I., 2000. Bacterioplankton distribution and production in deep Pacific waters: large-scale geographic variations and possible coupling with sinking particle fluxes. *Limnol. Oceanogr.* 45, 426–435. <https://doi.org/10.4319/lo.2000.45.2.0426>.
- Nguyen, T.T.H., Zakem, E.J., Ebrahimi, A., Schwartzman, J., Caglar, T., Amarnath, K., Alcolombri, U., Peaudecerf, F.J., Hwa, T., Stocker, R., Cordero, O.X., Levine, N.M., 2022. Microbes contribute to setting the ocean carbon flux by altering the fate of sinking particulates. *Nat. Commun.* 13, 1657. <https://doi.org/10.1038/s41467-022-29297-2>.
- Ogawa, H., Amagai, Y., Koike, I., Kaiser, K., Benner, R., 2001. Production of refractory dissolved organic matter by bacteria. *Science* 292, 917–920. <https://doi.org/10.1126/science.1057627>.
- Olli, K., 2015. Unraveling the uncertainty and error propagation in the vertical flux Martin curve. *Prog. Oceanogr.* 135, 146–155. <https://doi.org/10.1016/j.pocean.2015.05.016>.
- Omand, M.M., Govindarajan, R., He, J., Mahadevan, A., 2020. Sinking flux of particulate organic matter in the oceans: sensitivity to particle characteristics. *Sci. Rep.* 10, 5582. <https://doi.org/10.1038/s41598-020-60424-5>.
- Primeau, F., Press, A.I.N., Primeau, F., Press, A.I.N., 2006. On the variability of the exponent in the power law depth dependence of POC flux estimated from sediment traps. *Deep Sea Res. Part I* 53, 1335–1343. <https://doi.org/10.1016/j.dsr.2006.06.003>.
- Rees, M., Childs, D.Z., Ellner, S.P., 2014. Building integral projection models: a user's guide. *J. Anim. Ecol.* 83, 528–545. <https://doi.org/10.1111/1365-2656.12178>.
- Sellers, K.F., Borle, S., Shmueli, G., 2012. The COM-Poisson model for count data: a. <https://doi.org/10.1002/asmb.918>.
- Seymour, J.R., Seuront, L., Doubell, M.J., Mitchell, J.G., 2008. Mesoscale and microscale spatial variability of bacteria and viruses during a *Phaeocystis globosa* bloom in the

- Eastern English Channel. *Estuar. Coast. Shelf Sci.* 80, 589–597. <https://doi.org/10.1016/j.ecss.2008.09.011>.
- Seymour, J.R., Stocker, R., et al., 2009. Resource patch formation and exploitation throughout the marine microbial food web. *Am. Nat.* 173, E15. <https://doi.org/10.1086/593004>.
- Sohrin, R., Imazawa, M., Fukuda, H., Suzuki, Y., 2010. Full-depth profiles of prokaryotes, heterotrophic nanoflagellates, and ciliates along a transect from the equatorial to the subarctic central Pacific Ocean. *Deep Sea Res. Part II: Top. Stud. Oceanogr.* 57, 1537–1550. <https://doi.org/10.1016/j.dsr2.2010.02.020>.
- Stocker, R., Seymour, J.R., Samadani, A., Hunt, D.E., Polz, M.F., 2008. Rapid chemotactic response enables marine bacteria to exploit ephemeral microscale nutrient patches. *Proc. Natl. Acad. Sci. USA* 105, 4209–4214. <https://doi.org/10.1073/pnas.0709765105>.
- Sunagawa, S., Coelho, L.P., Chaffron, S., Kultima, J.R., Labadie, K., Salazar, G., Djahanschiri, B., Zeller, G., Mende, D.R., Alberti, A., Cornejo-castillo, F.M., Costea, P.I., Cruaud, C., Ovidio, F., Engelen, S., Ferrera, I., Gasol, J.M., Guidi, L., Hildebrand, F., Kokoszka, F., Lepoivre, C., 2015. Structure and function of the global ocean microbiome 348, 1–10.
- Tanaka, T., 2009. Structure and function of the mesopelagic microbial loop in the NW Mediterranean Sea. *Aquat. Microb. Ecol.* 57, 351–362. <https://doi.org/10.3354/ame01370>.
- TeamCore, R.C. 2018. R: A language and environment for statistical computing. R Foundation for Statistical Computing, Vienna, Austria.
- Tréguer, P., Bowler, C., Moriceau, B., Dutkiewicz, S., Gehlen, M., Aumont, O., Bittner, L., Dugdale, R., Finkel, Z., Iudicone, D., Jahn, O., Guidi, L., Lasbleiz, M., Leblanc, K., Levy, M., Pondaven, P., 2018. Influence of diatom diversity on the ocean biological carbon pump. *Nat. Geosci.* 11, 27–37. <https://doi.org/10.1038/s41561-017-0028-x>.
- Turley, C.M., Stutt, E.D., 2000. Depth-related cell-specific bacterial leucine incorporation rates on particles and its biogeochemical significance in the Northwest Mediterranean. *Limnol. Oceanogr.* 45, 419–425. <https://doi.org/10.4319/lo.2000.45.2.0419>.
- Urvoy, M., Labry, C., L'Helguen, S., Lami, R., 2022. Quorum sensing regulates bacterial processes that play a major role in marine biogeochemical cycles. *Front. Mar. Sci.* 9. <https://doi.org/10.3389/fmars.2022.834337>.
- Vadstein, O., Olsen, L., Andersen, T., 2012. Prey-predator dynamics in rotifers: density-dependent consequences of spatial heterogeneity due to surface attachment. *Ecology* 93, 1795–1801.
- Walters, C., 1997. Challenges in adaptive management of riparian and coastal ecosystems. *Conserv. Ecol.* 1.
- Wickman, J., Litchman, E., Klausmeier, C.A., 2024. Eco-evolutionary emergence of macroecological scaling in plankton communities. *Science* 383, 777–782. <https://doi.org/10.1126/science.adk6901>.
- Yamada, N., Fukuda, H., Ogawa, H., Saito, H., Suzumura, M., 2012. Heterotrophic bacterial production and extracellular enzymatic activity in sinking particulate matter in the western North Pacific Ocean. *Front. Microbiol.* 3. <https://doi.org/10.3389/fmicb.2012.00379>.
- Yang, Y., Motegi, C., Yokokawa, T., Nagata, T., 2010. Large-scale distribution patterns of virioplankton in the upper ocean. *Aquat. Microb. Ecol.* 60, 233–246. <https://doi.org/10.3354/ame01428>.
- Yang, Y., Yokokawa, T., Motegi, C., Nagata, T., 2014. Large-scale distribution of viruses in deep waters of the Pacific and Southern Oceans. *Aquat. Microb. Ecol.* 71, 193–202. <https://doi.org/10.3354/ame01677>.
- Yokokawa, T., Yang, Y., Motegi, C., Nagata, T., 2013. Large-scale geographical variation in prokaryotic abundance and production in meso- and bathypelagic zones of the central Pacific and Southern Ocean. *Limnol. Oceanogr.* 58, 61–73. <https://doi.org/10.4319/lo.2013.58.1.0061>.
- Yoneya, K., Miki, T., Van den Wyngaert, S., Grossart, H., Kagami, M., 2021. Non-random patterns of chytrid infections on phytoplankton host cells: mathematical and chemical ecology approaches. *Aquat. Microb. Ecol.* 87, 1–15. <https://doi.org/10.3354/ame01966>.